

# On the $P$ – $T$ – $fO_2$ stability of $Fe_4O_5$ , $Fe_5O_6$ and $Fe_4O_5$ -rich solid solutions

Robert Myhill<sup>1,3</sup>  · Dickson O. Ojwang<sup>1,2</sup> · Luca Ziberna<sup>1,3</sup> · Daniel J. Frost<sup>1</sup> · Tiziana Boffa Ballaran<sup>1</sup> · Nobuyoshi Miyajima<sup>1</sup>

Accepted: 10 April 2016

**Abstract** The high-pressure phases  $Fe_4O_5$  and  $Fe_5O_6$  have recently been added to the list of known iron oxides. As mixed-valence phases, it has been suggested that they could form in the Earth’s mantle once the dominant minerals become saturated in ferric iron. The possibility that  $Fe_4O_5$  could exist in the mantle is also supported by the fact that it forms extensive solid solutions with both  $Mg^{2+}$  and  $Cr^{3+}$ . In this study, we present the results of high-pressure and high-temperature multi-anvil experiments performed between 5 and 24 GPa at 1000–1400 °C aimed at constraining the stability field of the  $Fe_4O_5$  phase. We combine these results with published phase equilibria, equation of state and Fe–Mg partitioning data to estimate the thermodynamic properties of  $Fe_4O_5$ ,  $Fe_5O_6$  and the  $(Mg,Fe)_2Fe_2O_5$  solid solution. Using our thermodynamic model, the oxygen fugacity at which the high-pressure iron oxides become stable is calculated and the redox stability of  $(Mg,Fe)_2Fe_2O_5$  in an assemblage of olivine and pyroxene is calculated as a function of the bulk  $Fe/(Fe + Mg)$

ratio.  $Fe_4O_5$  and  $(Mg,Fe)_2Fe_2O_5$  are stable at oxygen fugacities higher than the diamond stability field and are, therefore, unlikely to be found as inclusions in diamonds. The stability field of  $Fe_5O_6$ , on the other hand, extends to oxygen fugacities compatible with diamond formation. Using the Mg–Fe solid solution model, we show that  $Fe_4O_5$ -structured phases would be restricted to aluminium-poor environments in the mantle such as dunites or silica–iron oxide-rich sediments transported into the mantle via subduction.

**Keywords**  $Fe_4O_5$  ·  $Fe_5O_6$  · Thermodynamics · Oxygen fugacity · Mantle · Deep Earth

## Introduction

The oxidation state of the Earth’s mantle has an important influence on many transport properties and is strongly related to the speciation of volatile elements with multiple oxidation states such as carbon (Wood et al. 1990; Ballhaus and Frost 1994; Frost and McCammon 2008). The oxygen fugacity of the Earth’s mantle affects the redox state of volcanic gases, for example, which in turn has influenced the availability of volatile elements at the surface over Earth’s history (Delano 2001). As such, understanding the past and present redox state of the mantle is an important goal. While oxy-thermobarometric methods can be applied to mantle xenoliths to estimate the oxygen fugacity within the top 200 km of the mantle (Wood et al. 1990; Wood 1991; Ballhaus et al. 1991; Stagno et al. 2013), the only samples currently available from greater pressures are mineral inclusions in diamonds. Although a wealth of information is now emerging concerning inclusions within so-called sublithospheric diamonds, estimating the redox conditions at which such minerals formed is difficult as redox

---

Communicated by Chris Ballhaus.

---

✉ Robert Myhill  
myhill.bob@gmail.com

<sup>1</sup> Bayerisches Geoinstitut, Universität Bayreuth, 95440 Bayreuth, Germany

<sup>2</sup> Inorganic and Structural Chemistry, Department of Materials and Environmental Chemistry, Arrhenius Laboratory, Stockholm University, 10691 Stockholm, Sweden

<sup>3</sup> School of Earth Sciences, University of Bristol, Wills Memorial Building, Queens Road, Bristol BS8 1RJ, UK

sensitive equilibria can rarely be identified. The presence of mixed-valence iron oxides as inclusions could provide an approximate indication of the oxygen fugacity prevailing in diamond-precipitating fluids in the mantle. For example, almost pure  $\text{Fe}_3\text{O}_4$  magnetite inclusions (Stachel et al. 1998; Kaminsky and Wirth 2011) have been found in diamonds, and evidence of  $(\text{Mg,Fe})\text{Fe}_2\text{O}_4$  exsolution from ferropicrinite (McCammon et al. 1998) has also been observed. Knowledge of the thermodynamic properties of iron oxides at high pressure is an important prerequisite for understanding the fluids in which such oxides form.

Recently, a new high-pressure mixed-valence phase with the stoichiometry  $\text{Fe}_4\text{O}_5$  has been reported as a breakdown product of siderite (Lavina et al. 2011) or magnetite (Woodland et al. 2012) at high pressures. Its crystal structure, determined mainly by powder diffraction and DFT calculations (Lavina et al. 2011; Trots et al. 2012; Guignard and Crichton 2014), has the orthorhombic *Cmcm* space group and consists of layers of edge-sharing  $\text{FeO}_6$  octahedra and layers of trigonal prisms alternating along the *c*-axis. With only 50 % of its iron in the trivalent state, this phase should be stable under more reducing conditions than magnetite. It is this property that makes  $\text{Fe}_4\text{O}_5$  a particularly interesting candidate as a potential host for ferric iron in the Earth’s mantle and as a possible gauge for redox processes.  $\text{Fe}_4\text{O}_5$ -structured phases can also accommodate  $\text{Mg}^{2+}$  and  $\text{Cr}^{3+}$ , which substitute for  $\text{Fe}^{2+}$  and  $\text{Fe}^{3+}$  (Woodland et al. 2013). This solid solution may have been missed in previous studies; for example, reanalysis of X-ray diffraction analysis of samples from  $\text{Mg}_2\text{SiO}_4$ – $\text{Fe}_2\text{SiO}_4$ – $\text{Fe}_3\text{O}_4$  experiments conducted by Koch et al. (2004) indicates the presence of  $(\text{Mg,Fe})_2\text{Fe}_2\text{O}_5$ . The isostructural end-member  $\text{Mg}_2\text{Fe}_2\text{O}_5$  was recently synthesized in high-pressure and high-temperature experiments (Boffa Ballaran et al. 2015). An  $\text{Fe}_2\text{Cr}_2\text{O}_5$  end member has also been synthesized (Ishii et al. 2014) although with a different octahedral stacking arrangement compared to  $\text{Fe}_4\text{O}_5$  and consequently a different space group (Ishii et al. 2014). A wide range of  $\text{M}_4\text{O}_5$  phase compositions (where M is a cation) may therefore be generated at high-pressure and high-temperature conditions through decomposition reactions involving spinel-structured phases.

A further high-pressure mixed-valence iron oxide with the stoichiometry  $\text{Fe}_5\text{O}_6$  has been recently reported by Lavina and Meng (2015). Formed between 10 and 20 GPa at  $\sim 2000$  °C, this phase apparently has the same orthorhombic space group as  $\text{Fe}_4\text{O}_5$  (*Cmcm*). In terms of oxygen fugacity, the stability field of  $\text{Fe}_5\text{O}_6$  should lie between wüstite and  $\text{Fe}_4\text{O}_5$ , and so this new phase may form even if there is insufficient oxygen in the system for  $\text{Fe}_4\text{O}_5$  to be stable.

Finally, several studies have reported that magnetite transforms to an orthorhombic structure, h- $\text{Fe}_3\text{O}_4$ ,

when compressed at room temperature to pressures above 19–27 GPa (Mao et al. 1974; Fei et al. 1999; Huang and Bassett 1986; Dubrovinsky et al. 2003). The stability field of h- $\text{Fe}_3\text{O}_4$  is not well known at high temperature, and sluggish kinetics at low temperatures leads to significant hysteresis (Fei et al. 1999; Lazor et al. 2004).

In this study, we investigate the stability of the high-pressure  $\text{Fe}_4\text{O}_5$  and  $\text{Fe}_5\text{O}_6$  phases. To this end, it is important to consider the following independent reactions:



Previous work has gone some way towards constraining the positions of these reactions. Schollenbruch et al. (2011), for example, conducted in situ experiments on magnetite starting compositions and observed a change in energy-dispersive X-ray diffraction patterns at 10–12 GPa which they attributed to the transformation of magnetite to its high-pressure polymorph (Reaction 4). However, they also observed additional peaks not attributable to h- $\text{Fe}_3\text{O}_4$ , which suggested the partial breakdown of  $\text{Fe}_3\text{O}_4$  to some unknown “mystery phase”. Unfortunately, the quality of their energy-dispersive diffraction patterns did not allow for structural or chemical determination of the phase. Woodland et al. (2012) conducted further in situ synchrotron experiments in the same region of *P*–*T* space and discovered that the reaction identified by Schollenbruch et al. (2011) was actually the breakdown of magnetite to  $\text{Fe}_4\text{O}_5$  and  $\text{Fe}_2\text{O}_3$  (Reaction 3).

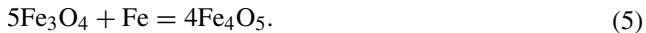
To examine the stability field of  $\text{Fe}_4\text{O}_5$ , we have performed high-pressure and high-temperature phase equilibria experiments in a multi-anvil apparatus. Using these results together with phase equilibria and compressibility data reported in the literature (Lavina et al. 2011; Schollenbruch et al. 2011; Woodland et al. 2013), we have extracted thermodynamic parameters to describe  $\text{Fe}_4\text{O}_5$  stability and that of the isostructural Mg-bearing solid solution  $(\text{Mg,Fe})_2\text{Fe}_2\text{O}_5$ . The available data on  $\text{Fe}_5\text{O}_6$  have also been employed to estimate its thermodynamic properties and stability field. Using the resulting models, the conditions at which such phases could form in the mantle are examined.

## Experimental and analytical methods

High-pressure and high-temperature experiments to examine the stability field of  $\text{Fe}_4\text{O}_5$  were conducted in a 500-tonne press using a Walker-type split-cylinder multi-anvil

module (Walker et al. 1990) and in 1000- and 1200-tonne presses using Kawai-type split-sphere guide blocks. For pressures up to 12 GPa, 18-mm edge length Cr<sub>2</sub>O<sub>3</sub>-doped MgO octahedra were employed as pressure media, which were compressed using tungsten carbide (WC) cubes with 11 mm corner truncations (a so-called 18/11 assembly). Higher-pressure experiments were performed using 14/8- and 10/4-type assemblies at 16 and 22 GPa, respectively. Each pressure medium contained a cylindrical LaCrO<sub>3</sub> or graphite furnace, placed inside an outer ZrO<sub>2</sub> sleeve. Further experimental details and pressure calibrations for all assemblies are reported by Keppler and Frost (2005). The temperature was monitored using W<sub>97</sub>Re<sub>3</sub>-W<sub>75</sub>Re<sub>25</sub> (D-type) thermocouples (with no correction made for the pressure effect on emf) inserted axially inside an alumina tube with the junction in contact with the top of the capsule. This set-up ensures that the temperature at the thermocouple junction is essentially identical to that at the top of the sample. We monitored the emf as a function of power during the experiments to check for reaction of the thermocouple. The stability of the emf with respect to the power drawn by the furnace under peak conditions suggests that there was no significant interaction between the thermocouple and the capsule.

A starting mix of magnetite and iron in a 5:1 molar ratio was used in all experiments, with high-pressure Fe<sub>4</sub>O<sub>5</sub> formation by the reaction



This mix was chosen to avoid complications involving the non-stoichiometry of wüstite (i.e. Fe<sub>1-y</sub>O where y ≠ 0). Magnetite was synthesized from high-purity Fe<sub>2</sub>O<sub>3</sub> (99.99 %) powder cold-pressed into pellets and reduced in a 1-atm CO-CO<sub>2</sub> gas-mixing furnace under controlled oxygen fugacity for 16 h at 1100 °C with CO<sub>2</sub>/CO ratio of 1.95/0.05, i.e. log *f*O<sub>2</sub> = -9.1 (Deines et al. 1974; Chou 1987). The product was ground in an agate mortar under ethanol with 6–9 μm Fe metal powder and then dried under a heat lamp before loading into cylindrical capsules made from 25-μm-thick folded metal foils. The metals used were Re or Mo, which impose different oxygen fugacities when in contact with their respective oxides (ReO<sub>2</sub> and MoO<sub>2</sub>). Capsule dimensions depended on the assemblies used: 2 mm Ø × 3.5 mm for the 18/11-type, 1.6 mm Ø × 2.5 mm for the 14/8-type and 1.2 mm Ø × 1.2 mm for the 10/4-type multi-anvil assemblies. Capsules were placed at the centre of the assembly within an MgO sleeve and were in contact, on one side, with the junction of the axially inserted thermocouple. Experiments were carried out at pressures between 5 and 22 GPa and temperatures between 1000 and 1400 °C. Run durations were between 2 and 20 h, after which the experiments were quenched by switching off the power to the furnace. Each experiment

**Table 1** Synthesis conditions and phases present in the run products identified by X-ray diffraction

Run Nr.	<i>P</i> (GPa)	<i>T</i> (°C)	<i>t</i> (hours)	Phase assemblage
V791	5	1100	5	Fe <sub>3</sub> O <sub>4</sub> + FeO
H3775	6	1000	3	Fe <sub>3</sub> O <sub>4</sub> + FeO
S5827	6	1250	3	Melt + Fe <sub>3</sub> O <sub>4</sub> + FeO
S5751	6	1100	5	Fe <sub>3</sub> O <sub>4</sub> + FeO
S5727 <sup>#</sup>	7	1000	5	Fe <sub>3</sub> O <sub>4</sub> + FeO + Mo-oxide
S5982	7	1100		Fe <sub>3</sub> O <sub>4</sub> + FeO
S5728 <sup>#</sup>	8	1100	5	Fe <sub>3</sub> O <sub>4</sub> + FeO + trace Fe <sub>4</sub> O <sub>5</sub> + Mo-oxide
V733	8	1300	3	Melt + Fe <sub>3</sub> O <sub>4</sub> + FeO
V734	8	1200	3	Fe <sub>3</sub> O <sub>4</sub> + Fe <sub>4</sub> O <sub>5</sub>
V743	8	1000	5.5	Fe <sub>3</sub> O <sub>4</sub> + Fe <sub>4</sub> O <sub>5</sub>
V736*	9	1200	7	Fe <sub>4</sub> O <sub>5</sub>
V744*	9	1000	5.5	Fe <sub>3</sub> O <sub>4</sub> + Fe <sub>4</sub> O <sub>5</sub>
S5698*	9	1000	20	Fe <sub>3</sub> O <sub>4</sub> + Fe <sub>4</sub> O <sub>5</sub>
H3551*	11	1000	7	Fe <sub>4</sub> O <sub>5</sub>
S5648*	12	1300	3	Fe <sub>4</sub> O <sub>5</sub> + ReO <sub>2</sub>
S5696*	12	1200	2	Fe <sub>4</sub> O <sub>5</sub> + ReO <sub>2</sub>
V739*	16	1100	3	Fe <sub>4</sub> O <sub>5</sub>
S5570*	16	1400	5	Fe <sub>4</sub> O <sub>5</sub>
S5640*	22	1000	5	Fe <sub>3</sub> O <sub>4</sub> + Fe <sub>4</sub> O <sub>5</sub>
S5646*	22	1200	4	Fe <sub>4</sub> O <sub>5</sub> + ReO <sub>2</sub>

V, H and S refer to experimental run numbers correspond to the 500, 1000 and 1200t multi-anvil presses, respectively. <sup>#</sup> Mo capsule. \* LaCrO<sub>3</sub> heaters. TEM analysis is conducted on Samples S5648 and S5696

was subsequently decompressed over several hours (see Table 1 for run details).

The starting material and the recovered run products were characterized by X-ray powder diffraction using a Philips X'Pert Pro X-ray diffraction system operating in reflection mode at 40 kV and 40 mA with CoKα<sub>1</sub> (λ = 1.78897 Å) radiation, monochromated with a symmetrically cut curved Johansson Ge<sub>(111)</sub> crystal, and equipped with a Philips X'celerator detector. The unit-cell edge of the magnetite starting material was *a*<sub>0</sub> = 8.3939 (6) Å, in perfect agreement with published values (e.g. Fleet 1982). The phases identified in the recovered run products are reported in Table 1. Forty to fifty per cent of each sample was ground for X-ray diffraction, so the phases reported are representative of the bulk material.

To determine accurately the unit-cell parameter of the Fe<sub>4</sub>O<sub>5</sub> phase, selected run products were mixed with Si (NBS standard material #640) as an internal standard. Full-pattern profile fitting (Rietveld analysis) was carried out on these samples using the GSAS software package (Larson and von Dreele 1988) and the Windows interface EXPGUI (Toby 2001). The resulting unit-cell parameters are reported in Table 2. Powder diffraction patterns of the

**Table 2** Unit-cell lattice parameters determined for Fe<sub>4</sub>O<sub>5</sub> synthesized at different pressures and temperatures

Run Nr.	Unit-cell lattice parameters Fe <sub>4</sub> O <sub>5</sub>			
	<i>a</i> (Å)	<i>b</i> (Å)	<i>c</i> (Å)	<i>V</i> (Å <sup>3</sup> )
V734	2.8925 (2)	9.8067 (9)	12.5791 (12)	356.82 (5)
V744	2.9008 (3)	9.7994 (7)	12.5772 (7)	357.53 (4)
S5696	2.8932 (3)	9.8040 (14)	12.5785 (17)	356.79 (6)

A small amount of Si is mixed with the sample and used as internal standard

Fe<sub>4</sub>O<sub>5</sub> phase exhibit relatively broad diffraction lines giving rise to uncertainties larger than those indicated by the GSAS program and reported in Table 2.

Three run products, H3551, V739 and S5570, were analysed exclusively by single-crystal X-ray diffraction. For this purpose, several crystals (more than 30 for each sample) were tested using an Xcalibur diffractometer with MoK $\alpha$  radiation operated at 50 kV and 40 mA, equipped with a CCD detector and a graphite monochromator. All crystals tested could be indexed with the Fe<sub>4</sub>O<sub>5</sub> unit cell, although they exhibited very broad peaks in the diffraction spectra (>0.3° in omega profiles).

In order to investigate the origin of the poor crystallinity shown by all Fe<sub>4</sub>O<sub>5</sub> single crystals examined, Sample S5648 was polished into a petrographic thin section with a thickness of 30  $\mu$ m. The thin section was glued onto a 3-mm-sized Mo grid and thinned to electron transparency by Ar-ion bombardment at an 8° angle of incidence and an accelerating voltage of 3.5 keV for 23 h. The crystals contained in the thin section were characterized by selected area electron diffraction (SAED), TEM imaging, electron diffraction and energy-dispersive X-ray (EDX) on a Philips CM20 FEG (field emission gun) STEM operating

at 200 keV. The NORAN Vantage EDX system includes a digital pulse processor, a Ge detector and ultra-thin window, enabling the detection of light elements such as oxygen.

## Thermodynamic framework

### Thermodynamic modelling of the Fe–O system

Thermodynamic data for Fe, Fe<sub>1-y</sub>O, Fe<sub>3</sub>O<sub>4</sub>, Fe<sub>4</sub>O<sub>5</sub> and Fe<sub>5</sub>O<sub>6</sub> are compiled and estimated using experimental data from this study and from the literature. Endmember data for BCC and FCC iron are taken from the 1 bar data of Sundman (1991) and equation of state of Komabayashi (2014). A subregular solid solution model was constructed for wüstite (Fe<sub>1-y</sub>O) with the end-member compositions [Fe<sup>2+</sup>]O and [Fe<sub>2/3</sub>□<sub>1/3</sub><sup>3+</sup>]O. Natural wüstite crystals usually have about 1/3 of the ferric iron cations in tetrahedral coordination, making an <sup>oct</sup>[Fe<sub>1/2</sub>□<sub>1/2</sub><sup>3+</sup>]tet[Fe<sup>3+</sup>]<sub>1/6</sub>O end member (Hazen and Jeanloz 1984), but as any constant ratio of octahedral/tetrahedrally coordinated Fe<sup>3+</sup> can be chosen to describe this end member without affecting the configurational entropy on the octahedral site, this complexity is ignored. We also ignore complex changes in defect structure that could affect compressional properties and therefore phase relations (e.g. McCammon and Liu 1984). In this study, we take the bulk modulus across the solid solution as a constant 152 GPa, which is suitable for more oxidized wüstites ( $y > 0.05$ ; McCammon 1993). The properties of the wüstite solid solution at 1 bar are obtained by fitting the  $fO_2$  across the wüstite solid solution (Bransky and Hed 1968; Giddings and Gordon 1973), and the compositions of wüstite in equilibrium with iron as a function of temperature. The resulting model (Table 3) has interaction

**Table 3** Thermodynamic data for FeO-, Fe<sub>4</sub>O<sub>5</sub>- and Fe<sub>5</sub>O<sub>6</sub>-structured phases

	Fe <sub>4</sub> O <sub>5</sub>	Fe <sub>5</sub> O <sub>6</sub>	Mg <sub>2</sub> Fe <sub>2</sub> O <sub>5</sub>	FeO	Fe <sub>2/3</sub> □ <sub>1/3</sub> O	h-Fe <sub>3</sub> O <sub>4</sub>
H <sub>0</sub> (J/mol)	-1.342e-6	-1.592e-6	-1.987e-6	-0.26545e-6	-0.25517e-6	-1.05746e-6
S <sub>0</sub> (J/K/mol)	230	290	169.0	58	38.5	172.4
V <sub>0</sub> (m <sup>3</sup> /mol)	5.376e-5	6.633e-5	5.305e-5	1.224e-5	1.107e-5	4.189e-5
K <sub>0</sub> (Pa)	1.857e-11	1.730e-11	1.700e-11	1.52e-11	1.52e-11	2.02e-11
K' <sub>0</sub> ()	4	4	4	4.9	4.9	4
K'' <sub>0</sub> (Pa <sup>-1</sup> )	-2.154e-11	-2.312e-11	-2.353e-11	-3.2e-11	-3.2e-11	-
$\alpha_0$ (K <sup>-1</sup> )	2.36e-5	1.51e-5	2.36e-5	3.22e-5	2.79e-5	3.59e-5
C <sub>p</sub> (J/K/mol)	306.9	351.3	284.9	42.64	54.63	262.5
	1.075e-3	9.355e-3	7.24e-4	8.971e-3	0.0	-7.205e-3
	3.1404e-6	-4.3546e-6	-3.3288e-6	-0.2608e-3	-0.7524e-6	-1.9262e-6
	-1.4705e-3	-1.2853e-3	-1.2560e-3	-0.1966e-3	-0.2192e-3	-1.6557e-3

Heat capacity parameters are in the form ( $a + bT + cT^{-2} + dT^{-0.5}$ ). h-Fe<sub>3</sub>O<sub>4</sub> from Lazor et al. (2004) is provided for completeness

parameters  $W(\text{FeO}-\text{Fe}_{2/3}\text{O}) = -40,121 + 4.27 T \text{ J/mol}$  and  $W(\text{Fe}_{2/3}\text{O}-\text{FeO}) = -4572 + 4.27 T \text{ J/mol}$ . It produces Gibbs energies of formation similar to those of Stølen and Grønvold (1996), with the added benefit that it can be trivially incorporated into existing solid solution data sets.

Thermodynamic parameters for magnetite and haematite are obtained from Dataset 6.2 of Holland and Powell (2011). Although the standard state enthalpy and entropy of these phases are derived from a different model for iron metal, the differences in Gibbs free energy are  $<1 \text{ kJ/mol}$ , which has a negligible effect on the work presented in this paper. The properties of  $\text{h-Fe}_3\text{O}_4$  are taken from Lazor et al. (2004).

Room temperature equations of state for the high-pressure iron oxides are compiled from the results of Lavina et al. (2011) and Woodland et al. (2012) for  $\text{Fe}_4\text{O}_5$ , and Lavina and Meng (2015) for  $\text{Fe}_5\text{O}_6$  (Table 3). The first derivative of the bulk modulus,  $K'$ , is fixed at 4, and the second derivative is fixed using the heuristic- $K'_0/K_0$  suggested by Holland and Powell (2011). To extrapolate the volumes to high temperature, we fit the standard state thermal expansivities of  $\text{Fe}_4\text{O}_5$  and  $\text{Fe}_5\text{O}_6$  to the single high  $P$ - $T$  data points reported by Woodland et al. (2012) and Lavina and Meng (2015). In the absence of heat capacity data, we use the molar sum of values from  $\text{FeO}$  (stoichiometric wüstite; Holland and Powell 2011) and magnetite, a technique proposed by Robinson and Haas (1983). Performing the same operation for magnetite using haematite and wüstite reproduces these  $C_p$  values to within a couple of per cent.

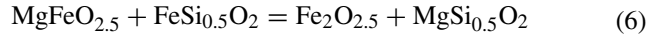
The standard state thermodynamic properties of  $\text{Fe}_4\text{O}_5$  can be determined either from the phase relations of Reaction (1) reported in this study or from Reaction (3) studied previously (Schollenbruch et al. 2011; Woodland et al. 2012). Here we use Reaction (3) to determine the standard state (1 bar, 298 K) enthalpy of formation and the entropy for  $\text{Fe}_4\text{O}_5$  and use reaction (1) purely to evaluate the prediction of the resulting model. Reaction (3) was tightly constrained by Schollenbruch et al. (2011), although at the time it was misidentified as the transformation from magnetite to its high-pressure polymorph (Woodland et al. 2012). The enthalpy and entropy thus obtained are given in Table 3.

Reactions related to the formation of  $\text{Fe}_5\text{O}_6$  are not yet well constrained. It appears that the phase becomes stable above  $\sim 10 \text{ GPa}$  at both 1200 and 1700 °C (Woodland et al. 2015; Lavina and Meng 2015), implying that Reaction (2) takes place at a pressure of 9–10 GPa, with a small  $dP/dT$ . The standard state enthalpy and entropy are chosen to satisfy these constraints. The small amount of data means that our thermodynamic model for  $\text{Fe}_5\text{O}_6$  must be considered preliminary. It may require adjustment as more data are published.

## Thermodynamic properties of the $\text{Fe}_4\text{O}_5$ - $\text{Mg}_2\text{Fe}_2\text{O}_5$ solid solution

For the purpose of assessing the stability of the  $(\text{Mg},\text{Fe}^{2+})_2\text{Fe}_2^{3+}\text{O}_5$  solid solution (Woodland et al. 2013; Boffa Ballaran et al. 2015), we make a first approximation of the thermodynamic properties of the  $\text{Mg}_2\text{Fe}_2\text{O}_5$  end member by examining  $\text{Fe}$ - $\text{Mg}$  partitioning data between  $(\text{Mg},\text{Fe}^{2+})_2\text{Fe}_2^{3+}\text{O}_5$  and  $(\text{Mg},\text{Fe})_2\text{SiO}_4$  solid solutions. In this analysis, it is assumed that  $\text{Fe}$ - $\text{Mg}$  ordering has little effect on the observed phase relations. The preference of  $\text{Mg}$  for the trigonal prism site of the  $(\text{Mg},\text{Fe}^{2+})_2\text{Fe}_2^{3+}\text{O}_5$  structure (Boffa Ballaran et al. 2015) suggests that this is not a perfect approximation, but is reasonable given the amount of data currently available.

The volume and bulk modulus of  $\text{Mg}_2\text{Fe}_2^{3+}\text{O}_5$  are taken from currently unpublished data (N. Siersch, pers. comm.). The volume  $V_0$  (5.305 J/bar/mol) is in good agreement with a Vegard's law analysis of the volumes of  $(\text{Mg},\text{Fe})_2\text{Fe}_2^{3+}\text{O}_5$  in Woodland et al. (2013). Woodland et al. (2013) also report compositions of coexisting  $(\text{Mg},\text{Fe}^{2+})_2\text{Fe}_2^{3+}\text{O}_5$  and  $(\text{Mg},\text{Fe})_2\text{SiO}_4$  olivine, wadsleyite and ringwoodite from experiments performed at 1100 °C between 9 and 16 GPa. These data have been used to constrain the properties of the solid solution. The exchange of  $\text{Fe}^{2+}$  and  $\text{Mg}$  between these phases can be described on a single-site mixing basis by the equilibrium,



The standard state Gibbs free energy for this equilibrium when the  $(\text{Mg},\text{Fe})_2\text{SiO}_4$  phase is olivine is described by,

$$\Delta G_{(P,T)}^\circ = -RT \ln \left( \frac{a_{\text{Fe}_2\text{O}_{2.5}}^{\text{oxide}} a_{\text{MgSi}_{0.5}\text{O}_2}^{\text{olivine}}}{a_{\text{MgFeO}_{2.5}}^{\text{oxide}} a_{\text{FeSi}_{0.5}\text{O}_2}^{\text{olivine}}} \right) \quad (7)$$

If we assume, based on the small difference in ionic radius between  $\text{Mg}$  and  $\text{Fe}^{2+}$ , that mixing is ideal in  $(\text{Mg},\text{Fe})_2\text{Fe}_2^{3+}\text{O}_5$ , then,

$$RT \ln \left( \frac{a_{\text{Fe}_2\text{O}_{2.5}}^{\text{oxide}} a_{\text{MgSi}_{0.5}\text{O}_2}^{\text{olivine}}}{a_{\text{MgFeO}_{2.5}}^{\text{oxide}} a_{\text{FeSi}_{0.5}\text{O}_2}^{\text{olivine}}} \right) = RT \ln \left( \frac{X_{\text{Fe}}^{\text{ox}} X_{\text{Mg}}^{\text{ol}}}{X_{\text{Mg}}^{\text{ox}} X_{\text{Fe}}^{\text{ol}}} \right) + W_{\text{Fe-Mg}}^{\text{ol}} \left( 2X_{\text{Fe}}^{\text{ol}} - 1 \right) \quad (8)$$

where, for example,  $X_{\text{Fe}}^{\text{ox}} = \text{Fe}^{2+}/(\text{Mg} + \text{Fe}^{2+})$  and  $W_{\text{Fe-Mg}}^{\text{ol}}$  is a Margules interaction parameter. In this study, we find the best-fitting standard state enthalpy of  $\text{Mg}_2\text{Fe}_2\text{O}_5$  from the observed compositions of coexisting olivine and  $(\text{Mg},\text{Fe})_2\text{Fe}_2\text{O}_5$  and then use this value to model the compositions of wadsleyite and ringwoodite coexisting with  $(\text{Mg},\text{Fe})_2\text{Fe}_2\text{O}_5$ .



## Results

### Microstructures in Fe<sub>4</sub>O<sub>5</sub>

Since all powder diffraction patterns and single-crystal diffraction profiles collected for Fe<sub>4</sub>O<sub>5</sub> exhibited broad diffraction lines, Sample S5648 (12 GPa, 1300 °C) was analysed by TEM in order to obtain some insight into the nature of defects present in this phase. Bright-field TEM images of the Ar-ion-milled sample show fringes of Fe<sub>4</sub>O<sub>5</sub> with fine parallel exsolution lamellae of Fe<sub>3</sub>O<sub>4</sub> (Fig. 1a). Indexing of the electron diffraction patterns revealed lamellar twinning of the magnetite phase. Magnetite crystals with numerous polysynthetic twins parallel to {311} are also observed in Sample S5640 (22 GPa, 1000 °C). The relationship between the two oxides is topotactic; the lattice planes {311} for Fe<sub>3</sub>O<sub>4</sub> and (002) for Fe<sub>4</sub>O<sub>5</sub> are coplanar, and the reciprocal spots in the selected area electron diffraction pattern are perpendicular to the plane of the lamellae (Fig. 1b). The presence of this lamellar intergrowth is likely to be the cause of the X-ray diffraction line broadening seen for Fe<sub>4</sub>O<sub>5</sub> profiles.

### Experimental phase relations of Fe<sub>4</sub>O<sub>5</sub>

The experimentally determined phase relations for Fe<sub>4</sub>O<sub>5</sub> (+ $\delta$ O) are shown in Fig. 2. Below ~8 GPa, the stable assemblage is a mixture of wüstite and magnetite. The Fe<sub>4</sub>O<sub>5</sub> formation reaction (1) was pressure-bracketed between 7 and 8 GPa at both 1000 and 1100 °C and temperature-bracketed between 1200 and 1300 °C at 8 GPa. The  $dP/dT$  slope of the transformation is therefore small, but probably slightly positive. The coexistence of Fe<sub>4</sub>O<sub>5</sub> and a small amount of magnetite at >8 GPa implies slight oxidation of the starting material, either prior to or during the experiment. The presence of twinned magnetite in run (S5640) from 22 GPa, discussed above, is most consistent with back-transformation with accompanying oxidation of Fe<sub>4</sub>O<sub>5</sub> during either decompression or grinding for powder X-ray diffraction analysis. As will be shown later, with respect to  $fO_2$ , the stability fields of both magnetite and Fe<sub>4</sub>O<sub>5</sub> are several log units higher than the Mo–MoO<sub>2</sub> oxygen buffer. This is consistent with the formation of small amounts of MoO<sub>2</sub> in both experiments where molybdenum capsules were employed. Similarly, the  $fO_2$  of the Re–ReO<sub>2</sub> buffer passes through the stability field of Fe<sub>4</sub>O<sub>5</sub>, which is consistent with the appearance of ReO<sub>2</sub> in experiments that used rhenium capsules.

At 1250 (6 GPa) and 1300 °C (8 GPa), a narrow corona of melt formed at the wall of the capsule around the wüstite plus magnetite assemblage (see Supplementary Figure 1). The melting points of both phases should be well over 1600 °C at this pressure (Lindsley 1966), and there is no eutectic between these phases, at least at 1 bar. The presence of Re metal within the quenched melt suggests that melting

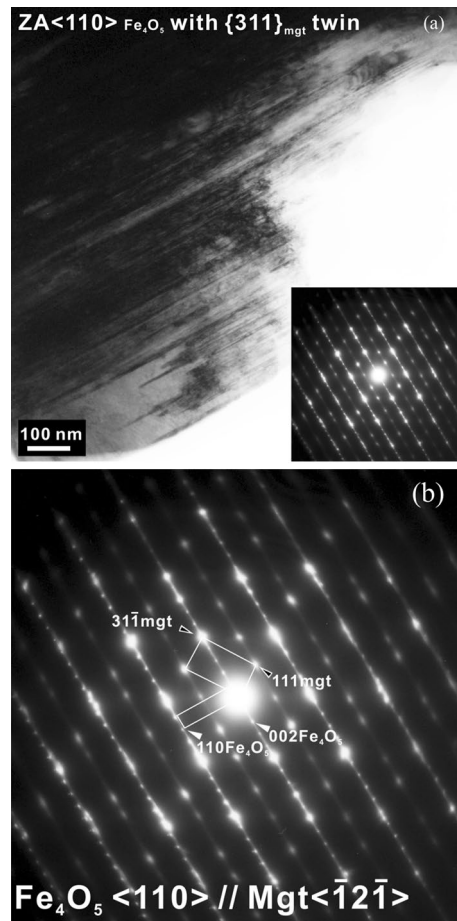


**Fig. 1** a Bright-field TEM image and corresponding electron diffraction pattern (*inset*) of Fe<sub>3</sub>O<sub>4</sub> and Fe<sub>4</sub>O<sub>5</sub> from run S5648. The images reveal the presence of nanometre-scale lamellae. b The same electron diffraction pattern as in (a), reproduced at a larger scale to clearly show the topotactic relationship between Fe<sub>3</sub>O<sub>4</sub> and Fe<sub>4</sub>O<sub>5</sub> phases. The electron diffraction pattern is taken across the lamellar-twin intergrowth imaged with the incident electron beam along  $\langle 110 \rangle$  and  $\langle \bar{1}2\bar{1} \rangle$  zone axes of Fe<sub>4</sub>O<sub>5</sub> and Fe<sub>3</sub>O<sub>4</sub>, respectively.

was fluxed by ReO<sub>2</sub>. Alternatively, hydrogen diffusion from the assembly driven by oxygen chemical potential gradients (e.g. Eugster 1957) could have caused the observed melting.

### Phase relations in the Fe–O system

A  $P$ – $fO_2$  diagram for the Fe–O system calculated at 1200 °C is shown in Fig. 3. The stabilities of the iron oxides are compared with curves calculated for the Re–ReO<sub>2</sub>, Mo–MoO<sub>2</sub>, EMOD (enstatite + magnetite = olivine + diamond), FMQ (fayalite = magnetite + quartz) and QIF (quartz + Fe = fayalite) oxygen buffers (Holland and Powell 2011; Holland et al. 2013). The metal–metal oxide buffer data are taken from Barin (1989) at 1 bar, with estimates for the PVT equations of state taken from the literature (see Supplementary Materials).

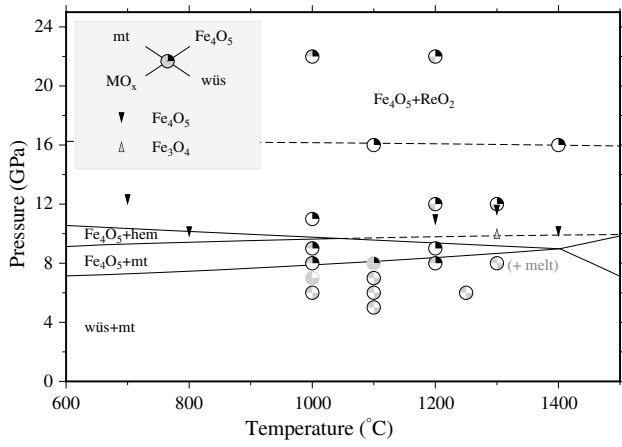


**Fig. 2** Isochemical  $P$ - $T$  phase diagram for the bulk composition  $\text{Fe}_4\text{O}_5 + \text{Re} + \delta\text{O}$ . The mineral assemblages observed in the run products of the high-pressure experiments (this study) are reported as wedges in the circular symbols. Triangular symbols indicate the reaction observed in situ by Schollenbruch et al. (2011) and identified as the magnetite-out reaction by Woodland et al. (2012). The solid lines correspond to univariant reactions calculated using the thermodynamic data described in the main text. The dashed black line corresponds to the part of the calculated  $\text{Fe}_3\text{O}_4 \rightarrow \text{Fe}_4\text{O}_5 + \text{Fe}_2\text{O}_3$  that is metastable at the  $\text{Re}-\text{ReO}_2$  buffer. The dashed grey line is the  $\text{Fe}_3\text{O}_4 \rightarrow \text{high Fe}_3\text{O}_4$  reaction (Lazor et al., 2004). We find high  $\text{Fe}_3\text{O}_4$  to be unstable relative to a mixture of  $\text{Fe}_4\text{O}_5 + \text{Fe}_2\text{O}_3$ .  $\text{MO}_x$  stands for the metal oxides of Re and Mo

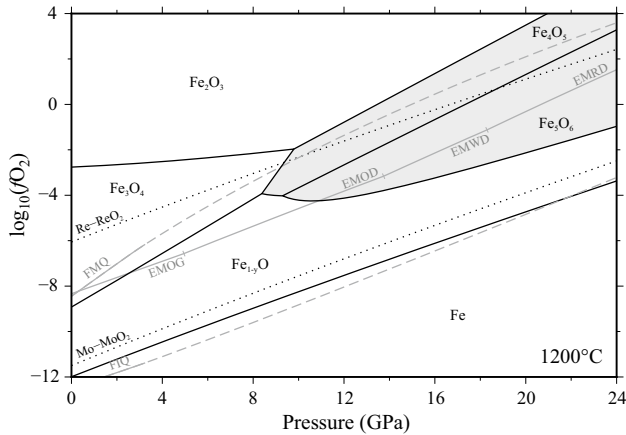


**Fig. 3** Stable phases in the  $\text{Fe}-\text{O}$  system as a function of pressure and oxygen fugacity at  $1200^\circ\text{C}$ . The black dotted lines correspond to the  $\text{Re}-\text{ReO}_2$ , and  $\text{Mo}-\text{MoO}_2$  buffers. The grey dashed lines are the (mostly) metastable QFM and QFI buffers. The solid grey lines delineate different regions of the stable QFM-/QFI-like buffers. The  $\text{Fe}_2\text{SiO}_4$  polymorphs are only stable within their labelled fields. Outside these fields, they will break down into iron/iron oxide and one of the  $\text{SiO}_2$  polymorphs

In appropriate bulk compositions,  $\text{Fe}_4\text{O}_5$  and  $\text{Fe}_5\text{O}_6$  are predicted to coexist over broad ranges of pressure and temperature, with the equilibrium between these iron oxides

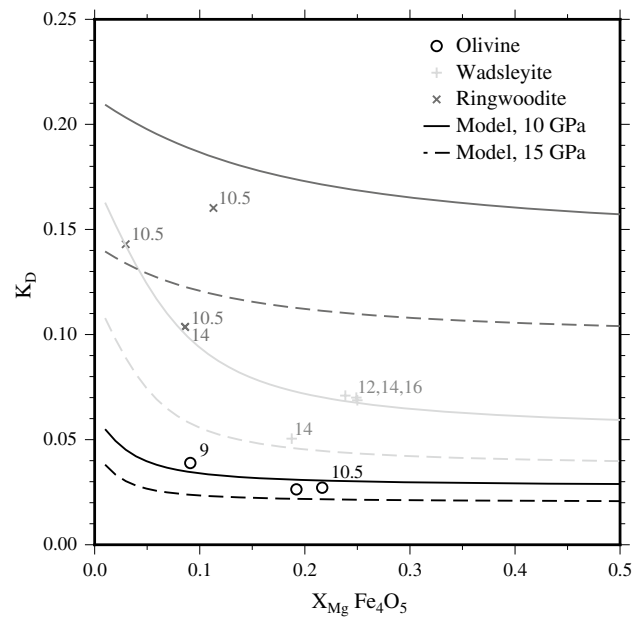


**Fig. 4** Mg content in  $(\text{Mg,Fe})_2\text{Fe}_2\text{O}_5$  versus the  $\text{Fe}/\text{Mg}$   $K_D$  with coexisting olivine polymorphs, taken from the data of Woodland et al. (2013). Experimental pressures in GPa are provided next to each data point. All data are collected at  $1100^\circ\text{C}$ . Curves show the fit of Eq. (7) using the parameters described in the text

lying 1–2 log units below the metastable extension of the FMQ buffer. The  $\text{Fe}_4\text{O}_5$  stability field is consistently above the EMOD buffer, implying that it is unlikely to be found as an inclusion within a mantle diamond.  $\text{Fe}_5\text{O}_6$ , on the other hand, is predicted to be stable within the forsterite + diamond stability field. The range of oxygen fugacities over which these mixed-valence iron oxides are stable expands with increasing pressure from  $\sim 3$  log units at 12 GPa to  $\sim 6$  log units at 21 GPa. The  $\text{Fe}_5\text{O}_6$  field expands mostly at the expense of the wüstite field. Although there are uncertainties in the model resulting from the fact that the formation pressure of  $\text{Fe}_5\text{O}_6$  is not well constrained as a function of temperature, this has little influence on the prediction that the wüstite field should narrow with pressure because this is a function of the volumes of the phases involved which are well constrained. Although the wüstite field narrows, the model predicts that at pressures higher than 24 GPa the wüstite- $\text{Fe}_5\text{O}_6$  and the wüstite-Fe boundary become essentially parallel in  $P$ - $f\text{O}_2$  space, ensuring that the wüstite stability field persists to high pressures, in accordance with experimental data (e.g. Ozawa et al. 2011).

### Equilibrium between $(\text{Fe,Mg})_2\text{Fe}_2\text{O}_5$ and the olivine polymorphs

Figure 4 shows the exchange coefficient  $K_D$  for equilibrium (6), where

$$K_D = \left( \frac{X_{\text{Fe}}^{\text{ox}} X_{\text{Mg}}^{\text{ol}}}{X_{\text{Mg}}^{\text{ox}} X_{\text{Fe}}^{\text{ol}}} \right) \quad (9)$$

plotted from the data of Woodland et al. (2013) as a function of the  $(\text{Mg},\text{Fe})_2\text{Fe}_2^{3+}\text{O}_5$   $\text{Mg}/(\text{Mg} + \text{Fe}^{2+})$  ratio for exchange with olivine, wadsleyite and ringwoodite. From fitting Eq. (7) to the data for olivine using values of  $W_{\text{Fe-Mg}}^{\text{ol}}$  from Holland et al. (2013), an estimate can be made for the standard state Gibbs free energy of equilibrium (6) at the  $P$ - $T$  conditions of the experiments. Using thermodynamic data for  $\text{Fe}_4\text{O}_5$  determined in this study and data on olivine from Holland et al. (2013), it is then possible to make an estimate of the Gibbs free energy of formation of  $\text{Mg}_2\text{Fe}_2^{3+}\text{O}_5$  at 1100 °C and 10 GPa. Finally, the formation of pure  $\text{Mg}_2\text{Fe}_2^{3+}\text{O}_5$  at 1550 °C, 15 GPa (Boffa Ballaran et al. 2015), constrains the standard state entropy to be at least 54 J/K/mol from the reaction  $\text{per} + \text{hem} \rightarrow \text{Mg}_2\text{Fe}_2^{3+}\text{O}_5$ .

As shown in Fig. 4, the resulting model provides an excellent fit to the olivine data, but there are discrepancies in calculated wadsleyite and ringwoodite compositions. We note that the equilibrium  $K_D$  values reported by Woodland et al. (2013) are rather scattered and do not exhibit the expected variation with pressure and Mg content. This may reflect disequilibrium or equilibration at different oxygen fugacities, which is known to influence Fe-Mg partitioning behaviour in wadsleyite and ringwoodite (Frost and McCammon 2009). Although Woodland et al. (2013) report very low ferric iron concentrations in their wadsleyites and ringwoodites, these are based on microprobe totals and therefore subject to quite large uncertainties which are heavily dependent on the analysed mineral phases and standards used for calibration.

## Discussion

### The breakdown of metastable $\text{Fe}_4\text{O}_5$

At room pressure,  $\text{Fe}_4\text{O}_5$  is a highly metastable phase prone to decomposition at relatively low temperatures (Trots et al. 2012). In this study, we show that  $\text{Fe}_4\text{O}_5$  breaks down under oxidizing conditions by forming lamellar intergrowths of {311}-twinned  $\text{Fe}_3\text{O}_4$ . We note that wüstite is not associated with the formation of this twinned magnetite, requiring bulk oxidation of the sample. The most likely explanation for our observations is that magnetite formed, while the sample was in contact with oxygen in the atmosphere or fluids used during preparation (epoxy, ethanol, water).

We also suggest that the unusual {311} twin in magnetite can be used to identify crystals which were once  $\text{Fe}_4\text{O}_5$ . We note that this form of twinning has been recognized in

magnetite coexisting with ringwoodite in samples recovered from quenched experiments performed at 21 GPa and 1600 °C by Frost et al. (2001), and in samples recovered from the high-pressure  $\text{Fe}_3\text{O}_4$  experiments conducted by Schollenbruch et al. (2011).

### The stability of $\text{Fe}_4\text{O}_5$ and implications for h- $\text{Fe}_3\text{O}_4$

The thermodynamic data for  $\text{Fe}_4\text{O}_5$  derived using experimental data on the magnetite-out reaction (Reaction 3) provide an excellent fit to the observed  $P$ - $T$  position of the  $\text{Fe}_4\text{O}_5$ -in reaction (Reaction 1; Fig. 2). The position of the magnetite-out reaction is very similar to the extrapolated  $\text{Fe}_3\text{O}_4 \rightarrow \text{h-Fe}_3\text{O}_4$  reaction proposed by Lazor et al. (2004). It is therefore important to discuss the stability of the high-pressure polymorph of magnetite.

Experimental investigations suggest that  $\text{Fe}_4\text{O}_5 + \text{Fe}_2\text{O}_3$  is more stable than h- $\text{Fe}_3\text{O}_4$  up to at least ~16 GPa at 1300 °C (Woodland et al. 2012). h- $\text{Fe}_3\text{O}_4$  has typically been investigated at much lower temperatures; for example, it was found to be stable relative to magnetite down to 24 GPa at 550 °C (Fei et al. 1999). Under these conditions, it is quite possible that the formation of  $\text{Fe}_4\text{O}_5 + \text{Fe}_2\text{O}_3$  may be kinetically hindered. The equation of state of h- $\text{Fe}_3\text{O}_4$  according to Lazor et al. (2004) indicates that the volume of h- $\text{Fe}_3\text{O}_4$  is consistently higher than that of  $0.5(\text{Fe}_4\text{O}_5 + \text{Fe}_2\text{O}_3)$  above ca. 200 °C, which would preclude h- $\text{Fe}_3\text{O}_4$  as a stable high-pressure, high-temperature phase. However, the equation of state of Lazor et al. lacks a Landau-type transition in high magnetite, which does exist in magnetite. This transition stabilizes magnetite at high temperature relative to h- $\text{Fe}_3\text{O}_4$ , explaining the discrepancy between the locations of the  $\text{Fe}_3\text{O}_4 \rightarrow \text{h-Fe}_3\text{O}_4$  reaction in this study (Fig. 2; 16 GPa at 900 °C) and in Lazor et al. (12 GPa at 900 °C). If high magnetite undergoes a Landau-type transition similar to that of its low-pressure polymorph, it does become stable at high temperature, but suggests that h- $\text{Fe}_3\text{O}_4$  is metastable relative to  $\text{Fe}_4\text{O}_5$  and  $\text{Fe}_2\text{O}_3$  at low temperature. Clearly, the high-temperature thermal properties of high magnetite (and  $\text{Fe}_4\text{O}_5$ ) are worthy of further study to better constrain the stability of h- $\text{Fe}_3\text{O}_4$ .

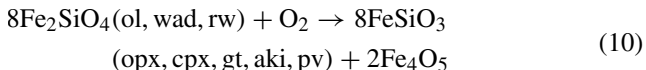
### The stability of $(\text{Mg},\text{Fe})_2\text{Fe}_2\text{O}_5$ relative to upper mantle phases

The compositions of upper mantle rocks generally place them within  $\pm 2$  log units of the FMQ oxygen buffer at low pressures (Frost and McCammon 2008). However, minerals such as clinopyroxene and garnet incorporate increasing quantities of ferric iron into their structures at higher pressures, which has the effect of decreasing the oxygen fugacity relative to the FMQ buffer (Rohrbach et al. 2007, 2011). Rocks from the deepest portions of the cratonic lithosphere record values that



are over 3 log units below FMQ (Stagno et al. 2013), and this trend is expected to result in the saturation of metallic iron in the deep upper mantle (Rohrbach et al. 2011).

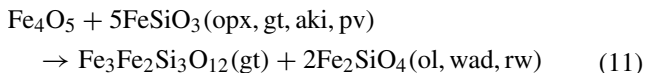
The upper mantle is comprised primarily of peridotitic rocks, which are not well described by the Fe–O system (Fig. 3). We extend our analysis to peridotitic assemblages by investigating the following redox reaction between the iron silicate end members of common mantle phases,



accounting for the fact that these minerals are solid solutions.

We first investigate the MgO–FeO–Fe<sub>2</sub>O<sub>3</sub>–SiO<sub>2</sub> (FMSO) system, which is the most mantle-like system under which Fe<sub>4</sub>O<sub>5</sub>-structured phases have been experimentally produced (Koch et al. 2004; Woodland et al. 2013). Figure 5 illustrates the effect of pressure on oxygen fugacity for an olivine–orthopyroxenite containing (Mg,Fe)<sub>2</sub>Fe<sub>2</sub>O<sub>5</sub> at 1400 °C. This diagram reveals that at high magnesium contents, (Mg,Fe)<sub>2</sub>Fe<sub>2</sub>O<sub>5</sub> is unstable relative to haematite. For example, a solid solution with 20–30 mol% Mg<sub>2</sub>Fe<sub>2</sub>O<sub>5</sub> in a peridotite with Mg/(Mg + Fe) ~0.9 imposes redox conditions that are more oxidizing than the (metastable) QFM buffer. The stabilization of (Mg,Fe)<sub>2</sub>Fe<sub>2</sub>O<sub>5</sub> in such a simple system would, therefore, require rocks which have remained isolated from mantle-derived fluids (which would impart lower oxygen fugacities on the system). However, the limited ability of olivine and HP-clinopyroxene to accommodate ferric iron means that these unusually high oxygen fugacities would not require unusually high ferric iron contents; primitive mantle typically has Fe<sup>3+</sup>/ΣFe ~ 0.03 (Canil et al. 1994).

The FMSO system accounts for the majority of mafic and ultramafic bulk compositions, but other components are also important for predicting high-pressure phase relations. Probably, the most important in this study is alumina, which stabilizes garnet, the dominant host of ferric iron in the deep upper mantle (Rohrbach et al. 2007, 2011). Even extremely depleted dunites contain non-negligible quantities of alumina in pyroxene and other minor phases (Godard et al. 2008). Unless (Mg,Fe)<sub>2</sub>Fe<sub>2</sub>O<sub>5</sub> solid solutions can also accept significant quantities of alumina, they will be destabilized by the following reaction:



Insights into the capacity of garnets to destabilize mixed-valence oxides can be gained from calculating the ferric iron contents of garnets at the oxygen fugacities where (Mg,Fe)<sub>2</sub>Fe<sub>2</sub>O<sub>5</sub> is stable. In Fig. 6, we calculate the ferric iron and pyrope content of FMSO garnets (White et al. 2014; updated version in the THERMOCALC database)

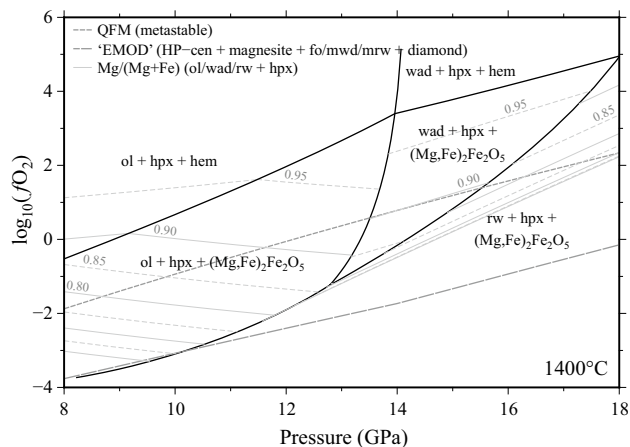


**Fig. 5** Modelled pressure– $f_{\text{O}_2}$  relations for (Mg,Fe)<sub>2</sub>SiO<sub>4</sub>–(Mg,Fe)<sub>2</sub>Si<sub>2</sub>O<sub>6</sub>–(Mg,Fe)<sub>2</sub>Fe<sub>2</sub>O<sub>5</sub> at 1400 °C. Compositional contours are molar Mg/(Mg + Fe) fractions in the ol + HP-cpx assemblage [i.e. the bulk Mg# when quantities of (Mg,Fe)<sub>2</sub>Fe<sub>2</sub>O<sub>5</sub> are negligible]. (Mg,Fe)<sub>2</sub>Fe<sub>2</sub>O<sub>5</sub> in the lower part of the diagram is metastable with respect to (Mg,Fe<sup>2+</sup>, Fe<sup>3+</sup>)O and potentially (Mg,Fe)<sub>3</sub>Fe<sub>2</sub>O<sub>6</sub>. Mg and Si solubility in haematite is ignored, as is the possibility of ferric iron-bearing spinels, which would exist between the haematite (hem) and (Mg,Fe)<sub>2</sub>Fe<sub>2</sub>O<sub>5</sub>-bearing fields. At the highest pressures, HP-clinopyroxene is metastable with respect to majoritic garnet. The “EMOD” (HP-clinoenstatite–magnesite–olivine/wadsleyite/ringwoodite–diamond) and metastable QFM (quartz–fayalite–magnetite) buffers are also shown

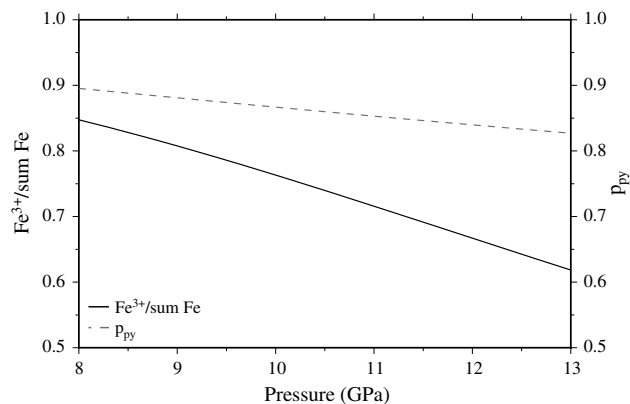


**Fig. 6** FMSO (py-alm-kho) garnet compositions corresponding to the 0.9 Mg/(Mg + Fe) contour in Fig. 5. Such ferric-rich compositions imply an extremely oxidized source (see discussion in text)

corresponding to the 0.9 Mg/(Mg + Fe) contour plotted in Fig. 5. The calculated ferric contents are extremely high; the formation of such khoharite-rich (Mg<sub>3</sub>Fe<sub>2</sub>Si<sub>3</sub>O<sub>12</sub>) garnets (and, by extension, (Mg,Fe)<sub>2</sub>Fe<sub>2</sub>O<sub>5</sub>) in normal alumina-bearing peridotite would require exceptionally oxygen-rich source rocks. The implication is that in the deep Earth, (Mg,Fe)<sub>2</sub>Fe<sub>2</sub>O<sub>5</sub> must be restricted to rocks with aluminium-poor bulk compositions.

We are currently unable to assess the potential stability of Fe<sub>5</sub>O<sub>6</sub>-structured phases in the mantle, as the stability of this phase will also depend on the extent and nature of the Mg-bearing solid solution and on the potential amount of alumina incorporation. If neither Fe<sub>4</sub>O<sub>5</sub> nor Fe<sub>5</sub>O<sub>6</sub> can substitute ferric iron for aluminium, their presence will be restricted to aluminium-poor lithologies, regardless of oxidation state.

## Conclusions

In this study, we have accurately constrained the stability of the new high-pressure phase Fe<sub>4</sub>O<sub>5</sub> under *P*–*T* conditions relevant to the upper mantle through multi-anvil experiments and subsequent analysis of run products. Microtextural analysis shows the quenched phase to be highly metastable and to display a lamellae intergrowth of magnetite that is likely formed during decompression or sample preparation. This probably explains the broad X-ray diffraction lines observed for this phase. Using the phase equilibria results, and those from previously published studies, we have constructed thermodynamic models to describe the stability of Fe<sub>4</sub>O<sub>5</sub> and Fe<sub>5</sub>O<sub>6</sub> and Mg-bearing Fe<sub>4</sub>O<sub>5</sub>. We use these models to calculate the oxygen fugacities at which these phases will be in equilibrium with other iron oxides and with mantle minerals.

The results show that the stabilization of (Mg,Fe)<sub>2</sub>Fe<sub>2</sub>O<sub>5</sub> within an assemblage containing olivine, olivine polymorphs and pyroxene requires oxygen fugacities >FMQ, which exceed those in the lithosphere, as estimated from mantle xenoliths (Stagno et al. 2013), and very likely those in the convecting mantle based on the iron redox state of mid-ocean ridge basalts (Cottrell and Kelley 2013). Furthermore, even if this oxygen fugacity were obtained, (Mg,Fe)<sub>2</sub>Fe<sub>2</sub>O<sub>5</sub> could only form if the bulk composition is extremely Al<sub>2</sub>O<sub>3</sub> depleted, otherwise unrealistically large bulk Fe<sup>3+</sup>/ΣFe ratios would be required. This would limit (Mg,Fe)<sub>2</sub>Fe<sub>2</sub>O<sub>5</sub> stability to lithologies such as highly oxidized dunites and sediments. It has been proposed that banded iron formations could have been subducted into the mantle in the Archean (Dobson and Brodholt 2005). Fe<sub>4</sub>O<sub>5</sub> would have very likely formed within such aluminium-poor lithologies as they reached pressures >8 GPa, providing that they did not interact with reducing fluids or melts.

Our modelling of the newly discovered phase Fe<sub>5</sub>O<sub>6</sub> suggests that it may be stable at mantle oxygen fugacities. However, we stress that there is currently very little experimental data on the end member and no data on solid solutions. In terms of determining whether this phase can exist in the mantle, a key issue will be to constrain the extent to which this phase forms solid solutions with Mg and Cr.

**Acknowledgments** This study was supported by a Humboldt Fellowship awarded to RM and the ERC Advanced Grant ACCRETE project (Contract Number 290568). The authors would like to thank Stefan Ubelhack and Heinz Fischer for assembly and capsule cutting and Hubert Schulze and Raphael Njul for the preparation of run products. They also thank Chris Ballhaus and two anonymous reviewers for their insightful comments which helped to significantly improve the manuscript.

## References

- Ballhaus C, Frost BR (1994) The generation of oxidised CO<sub>2</sub>-bearing basaltic melts from reduced CH<sub>4</sub>-bearing upper mantle sources. *Geochim Cosmochim Acta* 58:4431–4440
- Ballhaus C, Berry RF, Green DH (1991) High pressure experimental calibration of the olivine–orthopyroxene–spinel oxygen geobarometer: implications for the oxidation state of the upper mantle. *Contrib Miner Petrol* 107:27–40
- Barin I (1989) Thermochemical data of pure substances, vol VII. VCH, Weinheim, FRG
- Boffa Ballaran T, Uenver-Thiele L, Woodland AB (2015) Complete substitution of Fe<sup>2+</sup> by Mg in Fe<sub>4</sub>O<sub>5</sub>: the crystal structure of the Mg<sub>2</sub>Fe<sub>2</sub>O<sub>5</sub> end-member. *Am Mineral* 100:628–632
- Bransky I, Hed AZ (1968) Thermogravimetric determination of the composition–oxygen partial pressure diagram of wustite (Fe<sub>1–y</sub>O). *J Am Ceram Soc* 51:231
- Canil D, O'Neill HSC, Pearson DG, Rudnick RL, McDonough WF, Carswell DA (1994) Ferric iron in peridotites and mantle oxidation states. *Earth Planet Sci Lett* 123:205–220
- Chou IM (1987) Oxygen buffer and hydrogen sensor techniques at elevated pressures and temperatures. In: Ulmer GC, Barnes HC Jr (eds) *Hydrothermal experimental techniques*. Wiley, New York, pp 60–99
- Cottrell E, Kelley KA (2013) Redox heterogeneity in mid-ocean ridge basalts as a function of mantle source. *Science* 340:1314–1317
- Deines P, Nafziger RH, Ulmer GC, Woermann E (1974) T–fO<sub>2</sub> tables for selected gas mixtures in the C–H–O system at one atmosphere total pressure. *Coll Earth Miner Sci Bull Exp Station* 88:1–129
- Delano JW (2001) Redox history of the Earth's interior since 3900 Ma: implications for prebiotic molecules. *Orig Life Evol Biosph* 31:311–341
- Dobson DP, Brodholt JP (2005) Subducted banded iron formations as a source of ultralow-velocity zones at the core–mantle boundary. *Nature* 434:371–337
- Dubrovinsky LS, Dubrovinskaia NA, McCammon C, Rozenberg GK, Ahuja R, Osorio-Guillen JM, Dmitriev V, Weber H-P, Le Bihan T, Johansson B (2003) The structure of the metallic high-pressure Fe<sub>3</sub>O<sub>4</sub> polymorph: experimental and theoretical study. *J Phys: Condens Matter* 15:7697–7706
- Eugster HP (1957) Heterogeneous reactions involving oxidation and reduction at high pressures and temperatures. *J Chem Phys* 26:1760–1761
- Fei Y, Frost DJ, Mao HK, Prewitt CT, Häusermann D (1999) In situ structure determination of the high-pressure phase of Fe<sub>3</sub>O<sub>4</sub>. *Am Mineral* 84:203–206
- Fleet ME (1982) The structure of magnetite: two annealed natural magnetites, Fe<sub>3.005</sub>O<sub>4</sub> and Fe<sub>2.96</sub>Mg<sub>0.04</sub>O<sub>4</sub>. *Acta Crystallogr C* 40:1491–1493
- Frost DJ, McCammon CA (2008) The redox state of Earth's mantle. *Ann Rev Earth Planet Sci* 36:389–420
- Frost DJ, McCammon CA (2009) The effect of oxygen fugacity on the olivine to wadsleyite transformation: implications for remote

- sensing of mantle redox state at the 410 km seismic discontinuity. *Am Mineral* 94:872–882
- Frost DJ, Langenhorst F, Van Aken PA (2001) Fe–Mg partitioning between ringwoodite and magnesiowüstite and the effect of pressure, temperature and oxygen fugacity. *Phys Chem Miner* 28:455–470
- Giddings RA, Gordon RS (1973) Review of oxygen activities and phase boundaries in wüstite as determined by electromotive-force and gravimetric methods. *J Am Ceram Soc* 56(3):111–116
- Godard M, Lagabriele Y, Alard O, Harvey J (2008) Geochemistry of the highly depleted peridotites drilled at ODP Sites 1272 and 1274 (Fifteen-Twenty Fracture Zone, Mid-Atlantic Ridge): Implications for mantle dynamics beneath a slow spreading ridge. *Earth Planet Sci Lett* 267:410–425
- Guignard J, Crichton WA (2014) Synthesis and recovery of bulk  $\text{Fe}_4\text{O}_5$  from magnetite,  $\text{Fe}_3\text{O}_4$ . A member of a self-similar series of structures for the lower mantle and transition zone. *Mineral Mag* 78:361–371
- Hazen RM, Jeanloz R (1984) Wüstite ( $\text{Fe}_{1-x}\text{O}$ ): a review of its defect structure and physical properties. *Rev Geophys* 22:37–46
- Holland TJB, Powell R (2011) An improved and extended internally consistent thermodynamic dataset for phases of petrological interest, involving a new equation of state for solids. *J Metamorph Geol* 29:333–383
- Holland TJ, Hudson NF, Powell R, Harte B (2013) New thermodynamic models and calculated phase equilibria in NCFMAS for basic and ultrabasic compositions through the transition zone into the uppermost lower mantle. *J Petrol* 54:1901–1920
- Huang E, Bassett WA (1986) Rapid determination of  $\text{Fe}_3\text{O}_4$  phase diagram by synchrotron radiation. *J Geophys Res Solid Earth* 91(B5):4697–4703
- Ishii T, Kojitani H, Tsukamoto S, Fujino K, Mori D, Inaguma Y, Tsujino N, Yoshino T, Yamazaki D, Higo Y, Funakoshi K, Akaogi M (2014) High-pressure phase transitions in  $\text{FeCr}_2\text{O}_4$  and structure analysis of new post-spinel  $\text{FeCr}_2\text{O}_4$  and  $\text{Fe}_2\text{Cr}_2\text{O}_5$  phases with meteoritic and petrological implications. *Am Mineral* in press
- Kaminsky FV, Wirth R (2011) Iron carbide inclusions in lower-mantle diamond from Juina Barzil. *Can Mineral* 49:555–572
- Keppeler H, Frost DJ (2005) Introduction to minerals under extreme conditions. In: Miletich R (ed) *Mineral behaviour at extreme conditions EMU notes in mineralogy 7*. Eötvös University Press, Budapest, pp 1–30
- Koch M, Woodland AB, Angel RJ (2004) Stability of spinelloid phases in the system  $\text{Mg}_2\text{SiO}_4\text{--Fe}_2\text{SiO}_4\text{--Fe}_3\text{O}_4$  at 1100 °C and up to 10.5 GPa. *Phys Earth Planet Inter* 143:171–183
- Komabayashi T (2014) Thermodynamics of melting relations in the system Fe–FeO at high pressure: implications for oxygen in the Earth's core. *J Geophys Res Solid Earth* 119(5):4164–4177
- Larson AC, von Dreele RB (1988) GSAS General Structure Analysis System. LANSCE, MS-H805. Los Alamos National Laboratory, New Mexico, Report LAUR 86–748
- Lavina B, Meng Y (2015) Unraveling the complexity of iron oxides at high pressure and temperature: synthesis of  $\text{Fe}_5\text{O}_6$ . *Sci Adv* 1(5):e1400260
- Lavina B, Dera P, Kim E, Meng Y, Downs RT, Weck PF, Sutton SR, Zhao Y (2011) Discovery of the recoverable high-pressure iron oxide  $\text{Fe}_4\text{O}_5$ . *Proc Natl Acad Sci (PNAS)* 108:17281–17285
- Lazor P, Shebanova ON, Annersten H (2004) High-pressure study of stability of magnetite by thermodynamic analysis and synchrotron X-ray diffraction. *J Geophys Res Solid Earth* 109:B5
- Lindsley DH (1966) Pressure-temperature relations in the system  $\text{FeO--SiO}_2$ , vol 65. Year Book Carnegie Inst, Washington, DC, pp 226–230
- Mao HK, Takahashi T, Bassett WA, Kinsland GL, Merrill L (1974) Isothermal compression of magnetite to 320 KB. *J Geophys Res* 79(8):1165–1170
- McCammon C (1993) Effect of pressure on the composition of the lower mantle end member  $\text{Fe}_x\text{O}$ . *Science* 259:66–68
- McCammon CA, Liu LG (1984) The effects of pressure and temperature on nonstoichiometric wüstite,  $\text{Fe}_x\text{O}$ : the iron-rich phase boundary. *Phys Chem Miner* 10:106–113
- McCammon CA, Chinn IL, Gurney JJ, McCallum M (1998) Ferric iron content of mineral inclusions in diamonds from George Creek, Colorado determined using Mössbauer spectroscopy. *Contrib Miner Petrol* 133:30–37
- Ozawa H, Takahashi F, Hirose K, Ohishi Y, Hirao N (2011) Phase transition of FeO and stratification in Earth's outer core. *Science* 334(6057):792–794
- Robinson GR, Haas JL (1983) Heat capacity, relative enthalpy, and calorimetric entropy of silicate minerals; an empirical method of prediction. *Am Mineral* 68:541–553
- Rohrbach A, Ballhaus C, Golla-Schindler U, Ulmer P, Kamenetsky VS, Kuzmin DV (2007) Metal saturation in the upper mantle. *Nature* 449:456–458
- Rohrbach A, Ballhaus C, Ulmer P, Golla-Schindler U, Schönbohm D (2011) Experimental evidence for a reduced metal-saturated upper mantle. *J Petrol* 52:717–731
- Schollenbruch K, Woodland AB, Frost DJ, Wang Y, Sanehira T, Langenhorst F (2011) In situ determination of the spinel-post-spinel transition in  $\text{Fe}_3\text{O}_4$  at high temperature and pressure by synchrotron X-ray diffraction. *Am Mineral* 96:820–827
- Stachel T, Harris JW, Brey GP (1998) Rare and unusual mineral inclusions in diamonds from Mwadui, Tanzania. *Contrib Miner Petrol* 132:34–47
- Stagno V, Ojwang DO, McCammon CA, Frost DJ (2013) The oxidation state of the mantle and the extraction of carbon from Earth's interior. *Nature* 493:84–88
- Stølen S, Grønvold F (1996) Calculation of the phase boundaries of wüstite at high pressure. *J Geophys Res Solid Earth* 101:11531–11540
- Sundman B (1991) An assessment of the Fe–O system. *J Phase Equilib* 12(2):127–140
- Toby BH (2001) EXPGUI, a graphical user interface for GSAS. *J Appl Crystallogr* 34:210–213
- Trots DM, Kurnosov A, Woodland AB, Frost DJ (2012) The thermal breakdown of  $\text{Fe}_4\text{O}_5$  at ambient pressure. In: European mineralogical conference, vol 1, EMC2012-556-1
- Walker D, Carpenter MA, Hitch CM (1990) Some simplifications to multianvil devices for high-pressure experiments. *Am Mineral* 75:1020–1028
- White RW, Powell R, Holland TJB, Johnson TE, Green ECR (2014) New mineral activity–composition relations for thermodynamic calculations in metapelitic systems. *J Metamorph Geol* 32:261–286
- Wood BJ (1991) Oxygen barometry of spinel peridotites. In: Lindsley DH (ed) *Oxide minerals: petrologic and magnetic significance. Review in Mineralogy, 25:417–31*. Mineral. Soc. Am., Washington, DC p 508
- Wood BJ, Bryndzia LT, Johnson KE (1990) Mantle oxidation state and its relationship to tectonic environment and fluid speciation. *Science* 248:337–345
- Woodland AB, Frost DJ, Trots DM, Klimm K, Mezouar M (2012) In situ observation of the breakdown of magnetite ( $\text{Fe}_3\text{O}_4$ ) to  $\text{Fe}_4\text{O}_5$  and hematite at high pressures and temperatures. *Am Mineral* 97:1808–1811
- Woodland AB, Schollenbruch K, Koch M, Boffa Ballaran T, Angel RJ, Frost DJ (2013)  $\text{Fe}_4\text{O}_5$  and its solid solutions in several simple systems. *Contrib Miner Petrol* 166:1677–1686
- Woodland AB, Uenver-Thiele L, Boffa Ballaran T (2015) Synthesis of  $\text{Fe}_5\text{O}_6$  and the high-pressure stability of  $\text{Fe}^{2+}$ – $\text{Fe}^{3+}$ -oxides related to  $\text{Fe}_4\text{O}_5$ . *Goldschmidt Abstracts*